Fizika Nizkikh Temperatur, 2001, v. 27, No. 8, p. 835–844

Mesoscopic multiterminal Josephson structures. I. Effects of nonlocal weak coupling

M. H. S. Amin[1], A. N. Omelyanchouk[2], and A. M. Zagoskin[1,3]

[1] *D-Wave Systems Inc., 320-1985 W. Broadway, Vancouver, B.C., V6J 4Y3 Canada*

[2] *B. Verkin Institute for Low Temperature Physics and Engineering of the National Academy of Sciences of Ukraine, 47 Lenin Ave., Kharkov 61103, Ukraine*
E-mail: omelyanchouk@ilt.kharkov.ua

[3] *Physics and Astronomy Dept., The University of British Columbia, 6224 Agricultural Rd., Vancouver, B.C., V6T 1Z1, Canada*

Received March 15, 2001

We investigate nonlocal coherent transport in ballistic four-terminal Josephson structures (in which bulk superconductors (terminals) are connected through a clean normal layer, e.g., a two-dimensional electron gas). Coherent anisotropic superposition of macroscopic wave functions of the superconductors in the normal region produces phase slip lines ($2D$ analogs to phase slip centers) and time-reversal symmetry breaking $2D$ vortex states in it, as well as such effects as phase dragging and magnetic flux transfer. The tunneling density of local Andreev states in the normal layer is shown to contain peaks at the positions controlled by the phase differences between the terminals. We have obtain the general dependence of these effects on the controlling supercurrent/phase differences between the terminals of the ballistic mesoscopic four-terminal SQUID.

PACS: 74.80.Fp, 85.25.Cp, 85.25.Dq

1. Introduction

Multiterminal Josephson junctions [1,2] generalize the usual (two-terminal) Josephson junctions [3] to the case of weak coupling between several massive superconducting banks (terminals). Compared with two-terminal junctions, such systems have additional degrees of freedom and the corresponding set of control parameters, preset transport currents, and (or) applied magnetic fluxes. As a result, the current- or voltage-biased and the magnetic flux-driven regimes can be combined in one multiterminal microstructure.

One of the implementations of multiterminal coupling is a system of short, dirty microbridges going from a common center to separate massive superconductors. The theory of this kind of multiterminals was derived in [4,5] within the phenomenological Ginzburg–Landau scheme (Aslamazov and Larkin model [6]). This approach is valid for temperatures T near the critical temperature T_c and for the local case, when the characteristic spatial scale is larger then the coherence length $\xi_0 \sim \hbar v_F / T_c$. The stationary states and the dynamical behavior of the microbridge-type multiterminals have been studied for different microstructures, four-terminal SQUID controlled by the transport current, weakly coupled superconducting rings (see review of theoretical and experimental results in [7,8]).

The Josephson effect in mesoscopic weak links with direct conductivity (S–N–S junctions, ballistic point contacts) exhibits specific features [9,10] which are absent in conventional dirty microconstrictions near T_c [6]. As in normal metal mesoscopic structures [11], the electrodynamics of supercurrents in mesoscopic Josephson junctions is nonlocal. The supercurrent density depends on the spatial distribution of the superconducting order parameter at all points of the mesoscopic weak-link region. The coherent current flow is carried by the Andreev states [12] formed inside the weak link. A nonlocal nature of mesoscopic supercurrents was demonstrated by Heida et al. [13], investigating mesoscopic S–$2DEG$–S (superconductor–two dimensional electron gas–superconductor) Josephson junctions. They measured $2\Phi_0$ periodicity of the critical current instead of the standard Φ_0

($\Phi_0 = hc/2e$ is the magnetic flux quantum). A theory of this effect was developed in Refs. 14,15.

The present-day level of nanofabrication technology has made it possible to realize multiterminal mesoscopic Josephson junctions, similar to the 2-terminal junction studied in [13]. A microscopic theory of the mesoscopic ballistic Josephson multiterminals was derived in Ref. 16. It is valid for arbitrary temperatures $0 < T < T_c$ and describes the nonlocal coherent current states in the system. The effects of nonlocal coupling, such as phase dragging and magnetic flux transfer, were obtained in Ref. 17.

In the present paper we continue the study of quantum interference effects in mesoscopic multiterminals, which are related to the nonlocality of weak coupling. The paper consists of two parts. In first part (Article I) the effects of nonlocal coupling in mesoscopic multiterminal structures are studied. The general properties of Josephson multiterminals are described in Sec. 2. Section 3 gives the results concerning the current distribution and density of states inside weak link. In Sec. 3 we study properties of four-terminal SQUID which are specific to the mesoscopic case. In the second part (Article II) a superconducting phase qubit based on a mesoscopic multiterminal junction is proposed and investigated.

2. Mesoscopic four-terminal junction

System description

In a mesoscopic 4-terminal junction, bulk superconductors (terminals) are weakly coupled to each other through a clean two-dimensional normal metal layer ($2D$ electron gas), as is shown in Fig. 1. The pairs of terminals can be incorporated in bulk superconducting rings or in circuits with preset transport currents. In Fig. 2 we show two such configurations. The first one (Fig. 2,*a*) presents two superconducting rings, each interrupted by a Josephson junction, which are at the same time weakly coupled to each other. The second configuration (Fig. 2,*b*), combines a current (or voltage) biased junction and a flux driven junction in the ring. We call this configuration the four-terminal SQUID controlled by the transport current.

The state of the ith terminal S_i ($i = 1, \ldots, 4$) is determined by the phase φ_i of the complex off-diagonal potential $\Delta_0 \exp(i\varphi_i)$. The superconducting banks induce an order parameter Ψ in the normal metal region (shaded area in Fig. 1). Inside this mesoscopic, fully phase coherent weak link, the supercurrent density $\mathbf{j}(\boldsymbol{\rho})$ at point $\boldsymbol{\rho}$ depends *nonlocally* on the values of the induced order parameter Ψ at all points $\boldsymbol{\rho}'$. In turn, the order parameter $\Psi(\boldsymbol{\rho})$ depends on the phases φ_i. The total current I_i flowing into the ith terminal depends on the phases φ_j of all the banks and has the form [16]:

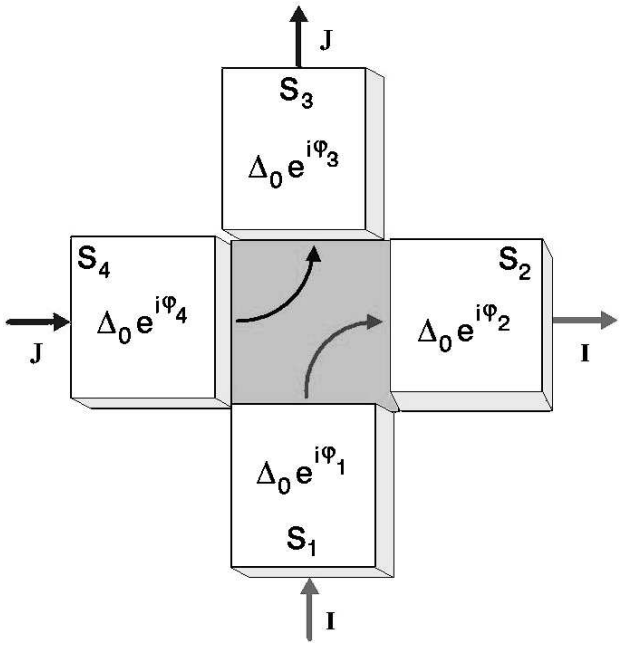

Fig. 1. Mesoscopic four-terminal Josephson junction with «parallel» implementation of the supercurrents. The four bulk superconducting regions, $S_1 \ldots S_4$, are weakly coupled through the thin layer of normal metal ($2DEG$), represented by the shaded area.

$$I_i = \frac{\pi\Delta_0}{e} \sum_{j=1}^{4} \gamma_{ij} \sin\left(\frac{\varphi_i - \varphi_j}{2}\right) \tanh\left[\frac{\Delta_0 \cos\left((\varphi_i - \varphi_j)/2\right)}{2T}\right]. \quad (1)$$

In the case of two terminals Eq. (1) reduces to the formula for ballistic point contacts [10] with γ_{12} equal to the Sharvin conductance.

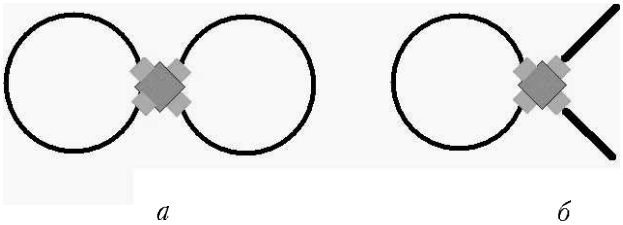

Fig. 2. Superconducting microstructures based on mesoscopic four-terminal Josephson junctions (*a*). Two weakly coupled superconducting rings (*b*). Mesoscopic four-terminal SQUID.

Expression (1) corresponds to the case of a small junction, when the linear dimensions of the N-layer are smaller than the coherence length $\xi \sim \hbar v_F / \Delta_0$ (for the case of arbitrary junction dimensions see Ref. 16). We are focusing here on the small junction case because the effects of nonlocality are most pronounced in this situation. The geometry dependent coefficients γ_{ij} denote the coupling between the partial Josephson currents in ballistic two-terminal S_i–S_j weak links.

Equation (1) is simplified when $T \approx 0$, or when $T \approx T_c$. In the $T = 0$ limit, it becomes

$$I_i = \frac{\pi\Delta_0(0)}{e} \sum_{j=1}^{4} \gamma_{ij} \sin\left(\frac{\varphi_i - \varphi_j}{2}\right) \operatorname{sign}\left[\cos\left(\frac{\varphi_i - \varphi_j}{2}\right)\right]. \tag{2}$$

Near T_c, on the other hand, the order parameter is small, $\Delta_0 \to 0$, and one can write

$$I_i = \frac{\pi\Delta_0^2(T)}{4eT_c} \sum_{j=1}^{4} \gamma_{ij} \sin(\varphi_i - \varphi_j). \tag{3}$$

Equations (2) and (3) are qualitatively similar, differing in the magnitude of critical currents and in the shape of the current-phase relations ($\sin(\varphi/2)\operatorname{sign}[\cos(\varphi/2)]$ and $\sin\varphi$). For definiteness, in the following we will consider the case $T \sim T_c$, keeping in mind that the results hold qualitatively at low temperatures as well.

For the Josephson coupling energy of the junction, E_J, which is related to the supercurrents I_i (3) through $I_i = (2e/\hbar)\partial E_J / \partial\varphi_i$, we have

$$E_J(\varphi_i) = \frac{\hbar}{2e} \frac{\pi\Delta_0^2(T)}{4eT_c} \sum_{j<k} \gamma_{jk} [1 - \cos(\varphi_j - \varphi_k)]. \tag{4}$$

Expression (1) for supercurrents I_i looks similar to Buttiker's multiprobe formula [18]

$$I_i = e \sum_j T_{ij}(\mu_i - \mu_j), \tag{5}$$

which relates the currents to the voltage drops between terminals in a mesoscopic normal metal multiterminal system. The similarity reflects the above-mentioned nonlocality of mesoscopic transport on a scale of $\xi_T \sim \hbar v_F / T$ (in the ballistic limit we are considering). The essential difference between (1) and (5) is that, unlike the Josephson currents of (1), the normal currents of (5) can flow only out of equilibrium; while the current-phase relation in (1) is periodic, the current–bias dependence of (5) certainly is not.

Circuit implementations of four-terminal junction. Nonlocal weak coupling

The current–phase relations (3) determine the behavior of the system in the presence of the transport currents and/or the diamagnetic currents induced by the magnetic fluxes through the closed superconducting rings. It is necessary to distinguish two types of circuit implementation of the mesoscopic 4-terminal junction [17]. The first one, is the «crossed» or «transverse» implementation, when the total current in one circuit goes in and out through one pair of opposite banks in Fig. 1, and in the second circuit — through the other pair. In the «parallel» implementation, shown in Fig. 1, the currents I and J flow through pairs of adjacent banks. In this case, nonlocal coupling of currents inside the mesoscopic N-layer results in the peculiar effect of «dragging» of the phase difference between one pair of terminals by the phase difference between another pair of terminals [17]. In the following, we consider the «parallel» implementation and study the manifestations of the phase dragging effect.

The coefficients γ_{ij} in (3), (4) depend on the geometry of the weak link (the shape of the N-layer) and on the transparency of S–N interfaces. In general we have $\gamma_{ij} = \gamma_{ji}$ and $\gamma_{ii} = 0$. For the case of parallel implementation, the elements γ_{12} and γ_{34} are related to the critical currents of the individual subjunctions S_1–S_2 and S_3–S_4, respectively. The matrix

$$\hat{\gamma}_{\text{coupl}} = \begin{pmatrix} \gamma_{13} & \gamma_{14} \\ \gamma_{23} & \gamma_{24} \end{pmatrix} \tag{6}$$

describes the coupling between these two junctions. The properties of the system (in particular, the existence of phase dragging) qualitatively depends on whether $\det(\hat{\gamma}_{\text{coupl}})$ is equal to zero or not (see Appendix). In the case of a conventional nonmesoscopic 4-terminal Josephson junction the coefficients γ_{ij} factorize, $\gamma_{ij} \sim (1/R_i)(1/R_j)$, where R_i are the normal resistances of the dirty microbridges [7]. This yields $\det(\hat{\gamma}_{\text{coupl}}) \equiv 0$, which we call local coupling. On the other hand, in a mesoscopic system, even in the completely symmetric case of an $a \times a$ square N-layer and ideal transparency ($D = 1$) of the N–S_i interfaces, the coefficients γ_{ij} are given by [17]:

$$\gamma_{12} = \gamma_{34} = \gamma_0 , \quad \hat{\gamma}_{\text{coupl}} = \gamma_0 \begin{pmatrix} \sqrt{2} & 1 \\ 1 & \sqrt{2} \end{pmatrix}, \qquad (7)$$

$$\gamma_0 = \frac{e^2 p_F a}{\sqrt{2}\,\hbar^2\pi^2} \left(1 - \frac{1}{\sqrt{2}}\right),$$

with $\det(\hat{\gamma}_{\text{coupl}}) \neq 0$. In a more general case than the completely symmetric one (Eq. (7)), we can write γ_{ij} in the form

$$\gamma_{34} = \kappa\gamma_{12} , \quad \hat{\gamma}_{\text{coupl}} = \gamma_0 \begin{pmatrix} p & q \\ q & p \end{pmatrix}. \qquad (8)$$

This corresponds to a square N-layer with different transparencies for junctions S_1–S_2 and S_3–S_4 and/or with different widths of the superconductor banks connected to the normal layer. In our numerical calculations we will use the simple form (7), i.e., $\kappa = 1$, $p = \sqrt{2}$, $q = 1$.

Current-phase relations. The phase dragging effect

Let us introduce the new variables:

$$\varphi_2 - \varphi_1 = \theta , \quad \varphi_3 - \varphi_4 = \phi ,$$

$$\frac{1}{2}(\varphi_1 + \varphi_2) = \alpha , \quad \frac{1}{2}(\varphi_4 + \varphi_3) = \beta , \qquad (9)$$

$$\alpha - \beta = \chi , \quad \alpha + \beta = \gamma .$$

Without loss of generality, we can choose the phase γ equal to zero ($\sum_j \phi_j = 0$). For the circuit implementation shown in Fig. 1, we have

$$I = I_2 = -I_1 , \; J = I_3 = -I_4 . \qquad (10)$$

In terms of the phase differences (9) the currents I and J have the form

$$I = \sin\theta + \left[(p+q)\sin\frac{\theta}{2}\cos\frac{\phi}{2} + (p-q)\cos\frac{\theta}{2}\sin\frac{\phi}{2}\right]\cos\chi , \qquad (11)$$

$$J = \kappa\sin\phi + \left[(p+q)\sin\frac{\phi}{2}\cos\frac{\theta}{2} + (p-q)\cos\frac{\phi}{2}\sin\frac{\theta}{2}\right]\cos\chi . \qquad (12)$$

All the γ's (8) are normalized by γ_{12}, and the currents I, J are measured in units of $I_0 = \pi\gamma_{12}\Delta_0^2(T)/4eT_c$.

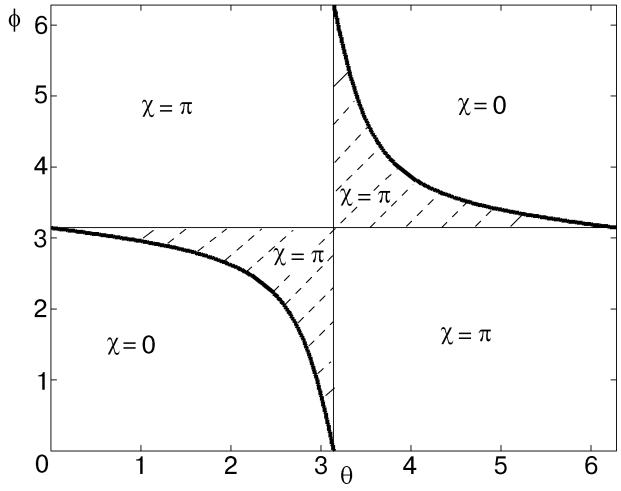

Fig. 3. Phase diagram for the phase difference χ in the (θ, ϕ) plane. Solid line separates the regions with $\chi = 0$ and $\chi = \pi$. The dashed region is absent in the case of local coupling.

From the current conservation (Eq.(10)), it follows that the phase χ in Eqs. (11) and (12) can take only two values, 0 or π. Minimization of E_J (4) with respect to χ also gives $\chi = 0$ or π, depending on the equilibrium values of θ and ϕ (see Appendix):

$$\cos\chi = \text{sign}\left[(p+q)\cos\frac{\phi}{2}\cos\frac{\theta}{2} - (p-q)\sin\frac{\phi}{2}\sin\frac{\theta}{2}\right]. \qquad (13)$$

The current–phase relations (11) and (12) with the condition (13) are invariant under the transformation $\theta \to \theta + 2\pi n$, and $\phi \to \phi + 2\pi k$. The 2π periodicity of observable quantities is sustained by the «hidden» variable phase χ. In Fig. 3 the phase diagram for χ in the (θ, ϕ) plane is presented. The solid line separates the regions with $\chi = 0$ and $\chi = \pi$. When the state of the system (θ, ϕ) crosses this line, a jump in χ occurs. Corresponding jumps take place in current–phase relations (11) and (12). The current $I(\theta)$ (11) is shown in Fig. 4 for several values of the phase ϕ. Note that the function $I(\theta)$ has jumps, which for $\phi \neq 0$, are not located at $\theta = \pm\pi$, as they would be in conventional 4-terminal junctions. The jump in χ means the slippage of the phase θ (or ϕ). In the case of two-terminal or conventional 4-terminal junction the phase-slip events occur at phase difference equal to $\pi(2n + 1)$, $n = 0, \pm 1, \pm 2, \ldots$ In one-dimensional structures slippage of the phase occurs at phase-slip centers (PSC), i.e., points where the order parameter equals zero. In our case of a $2D$ mesoscopic 4-terminal weak link, the analog of the PSC are phase-slip lines in the normal metal region. They appear when the state (θ, ϕ) of the system belongs to the dashed

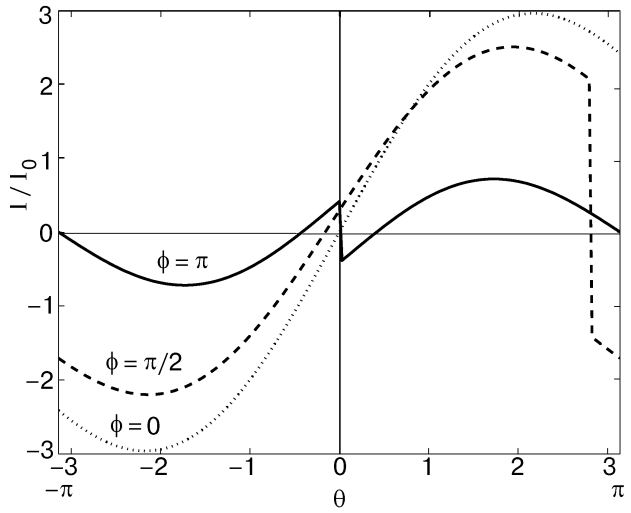

Fig. 4. Current–phase relations I for different values of ϕ.

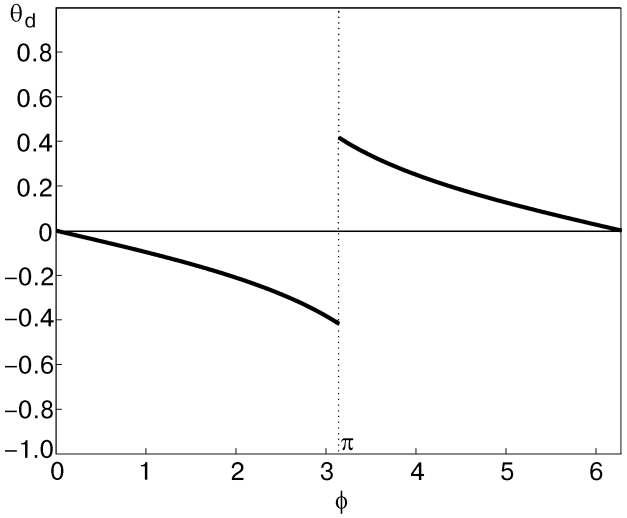

Fig. 5. The dragged phase θ_d between terminals S_1–S_2, at zero transport current I, as a function of the phase difference ϕ between the other pair of terminals S_3–S_4.

region in Fig. 3. This region, which is absent in the local coupling case (it actually coincides with the lines $\theta = \pi$, $\phi = \pi$), we call the «frustrated» region for phases θ and ϕ. For states inside this region, the distribution of the supercurrent in the weak link contains $2D$ vortex states (see below).

Nonlocal weak coupling leads to the phase dragging effect [17]. One notices that if $p \neq q$ then putting $\theta = 0$ in (11) results in a nonzero value of the current I:

$$I = (p - q) \sin\frac{\phi}{2} \operatorname{sign}\left(\cos\frac{\phi}{2}\right). \qquad (14)$$

This current is absent in conventional 4-terminal junctions or mesoscopic four-terminal junctions with crossed implementation at which $p = q$ (i.e., $\det(\hat{\gamma}_{\mathrm{coupl}}) = 0$).

Similarly, if we set $I = 0$ in (11), we find a nonzero solution for θ, which again vanishes when $p = q$. This solution ($\equiv \theta_d$) is a function of ϕ and is plotted versus ϕ in Fig. 5. The influence of the phase of one side of the mesoscopic 4-terminal junction on the phase of the other side is what we call the phase dragging effect. This effect is one of the important characteristics of the junction with parallel implementation.

In general the current–phase relations are asymmetric, $I(-\theta) \neq -I(\theta)$, unlike in conventional cases. In another words, the presence of a phase difference ϕ on the terminals S_4–S_3 breaks the time reversal symmetry for the Josephson junction S_1–S_2. It also follows from expression (11) that $I(\theta)$ is not only a function of $|\phi|$, as in conventional junctions, but also depends on the sign of ϕ. The phase dragging has an analog in the normal metal mesoscopic multiterminals described by formula (5); the normal current flowing through one pair of terminals induces a voltage difference between the other ones [18].

3. Current distribution and local density of states inside the mesoscopic weak link

The coupling through the normal layer determines the behavior of the Josephson weak links S_1–S_2 and S_4–S_3. On the other hand, the properties of the normal layer itself depend on the phase differences θ and ϕ across the junctions. The phases θ and ϕ can be controlled by external magnetic fluxes through the rings (Fig. 2,*a*). In this section we present the results of numerical calculations for the current density distribution $\mathbf{j}(\boldsymbol{\rho})$ and density of local Andreev levels $N(\epsilon)$ inside the mesoscopic 4-terminal weak link. The expressions for $\mathbf{j}(\boldsymbol{\rho})$ and $N(\epsilon)$ as functionals of $\{\varphi_1, \varphi_2, \varphi_3, \varphi_4\}$ were obtained in Ref. 16 by solving the Eilenberger equations [19].

Figure 6 illustrates the effect of phase dragging. Two sets of phases ($\theta = -0.42$, $\phi = \pi$) and ($\theta = 0.42$, $\phi = \pi$) correspond to zero value of the current I (11) (see Fig. 4) and opposite directions of the current J (12). In the absence of the current from terminal S_1 to terminal S_2, a phase difference across the junction S_1–S_2 exists.

When the phases θ and ϕ lie in the «frustrated» region of the diagram Fig. 3 (dashed area), the current distribution $\mathbf{j}(\boldsymbol{\rho})$ contains $2D$ vortex states. They are shown in Fig. 7 for states ($\theta = \pi - 0.2$, $\phi = \pi - 0.2$) and ($\theta = \pi + 0.2$, $\phi = \pi + 0.2$). In both cases, the order parameter $\Psi(\boldsymbol{\rho})$ vanishes along the diagonal $x = y$, and its phase drops by π when crossing this $2D$ phase-slip line.

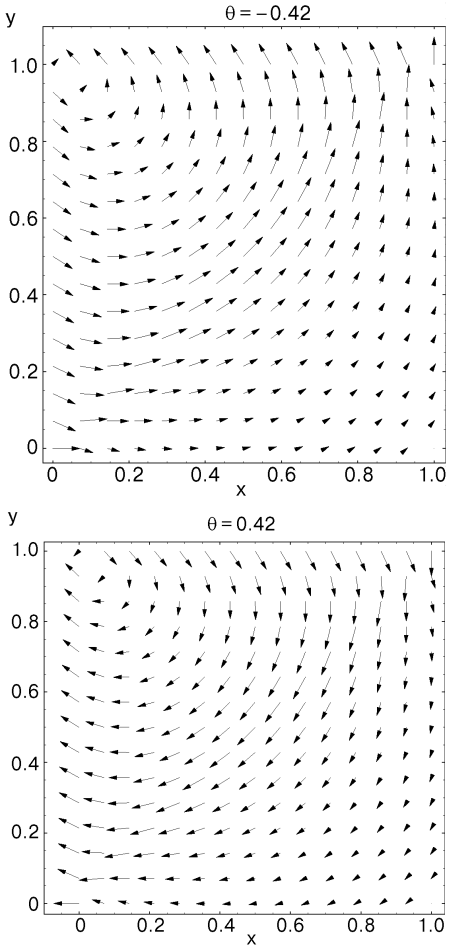

Fig. 6. Distribution of the current density inside the normal layer for phase $\phi = \pi$ and two values of the phase θ at which the current $I = 0$ (Fig. 4).

The Andreev scattering processes on the S_i–N interfaces lead to the appearance of energy levels with energies ϵ inside the gap Δ_0, $|\epsilon| < \Delta_0$, in the normal metal. The local density of electron states in the normal layer is given by the formula

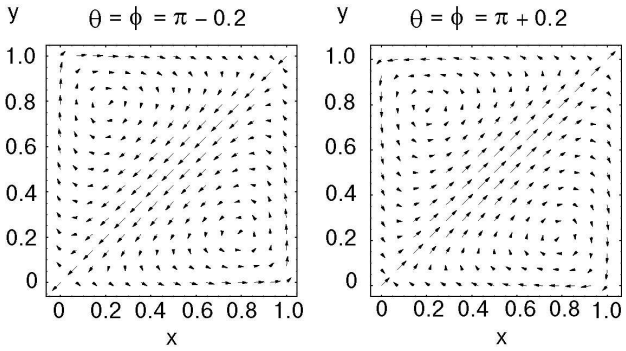

Fig. 7. The vortex-like distributions of the current inside the weak link when θ and ϕ are inside the frustrated region.

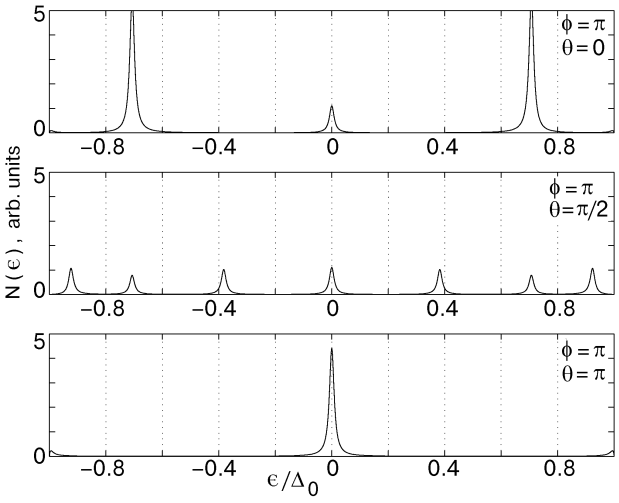

Fig. 8. Density of states, $N(\epsilon)$, averaged over the normal region for different values of θ and ϕ.

$$\mathcal{N}(\epsilon, \rho) = N(0) \langle \mathrm{Re}\, g(\omega = -i\epsilon, \rho, \mathbf{v}_F) \rangle_{\mathbf{v}_F} . \quad (15)$$

($g(\omega, \rho, \mathbf{v}_F)$ is the Eilenberger Green's function). We have studied the dependence of the density of states, averaged over area of the N-layer, $N(\epsilon)$, on the phases θ and ϕ. This tunneling density of states can be measured by a scanning tunneling microscope. It contains the spikes with intensity and position on the energy axes controlled by the phases θ and ϕ. The results are shown in Fig. 8 (the δ-function singularities in $N(\epsilon)$ are smeared by introducing a small damping $\Gamma = 0.01\Delta_0$).

4. Mesoscopic four-terminal SQUID

In this section we consider the four-terminal SQUID configuration (Fig. 2,*b*). The conventional 4-terminal SQUID has been studied in detail in Ref. 5, wherein the steady-state domain and dynamical properties of the system were calculated. Here we are interested in the specific features of the mesoscopic case reflected in the current–phase relations (11), (12). As we have seen in the previous Section, the nonlocal coupling ($p \neq q$) leads to the phase dragging effect. This dragged phase can induce in the ring a transferred magnetic flux which depends on the transport current. Conversely the magnetic flux state in the ring influences the behavior of the Josephson junction in the current circuit.

When the terminals 3 and 4 are short-circuited by a superconducting ring with self-inductance L, the phase ϕ is related to the observable quantity, the magnetic flux Φ threading the ring $\phi = (2e/\hbar)\Phi$. The current J circulating in the ring is

given by $J = (\Phi^e - \Phi)/L$, where Φ^e is the external magnetic flux threading the ring. From (11) and (12) we have

$$I = \sin\theta + \left[(p+q)\sin\frac{\theta}{2}\cos\frac{\Phi}{2} + (p-q)\cos\frac{\theta}{2}\sin\frac{\Phi}{2}\right]\cos\chi\,, \tag{16}$$

$$\frac{\Phi^e - \Phi}{\mathcal{L}} = \sin\Phi + \frac{1}{\kappa}\left[(p+q)\sin\frac{\Phi}{2}\cos\frac{\theta}{2} + (p-q)\cos\frac{\Phi}{2}\sin\frac{\theta}{2}\right]\cos\chi\,, \tag{17}$$

where the fluxes Φ, Φ^e are measured in units $\hbar/2e$, and $\mathcal{L} = (2e/\hbar)LI_0\kappa$ is the dimensionless self-inductance. The parameter $\kappa = \gamma_{34}/\gamma_{12}$ is the ratio of the critical currents of the subjunctions 3–4 and 1–2. The limiting cases of $\kappa \to \infty$ and $\kappa \to 0$ correspond to the autonomous SQUID and the current-biased Josephson junction, respectively.

The transport current I and the external flux Φ^e are the external control parameters. The corresponding Gibbs potential for the 4-terminal SQUID takes the form

$$U(\Phi, \theta;\, I, \Phi^e) = \frac{\kappa(\Phi - \Phi^e)^2}{2\mathcal{L}} - I\theta - \cos\theta - \kappa\cos\Phi - 2\left[(p+q)\cos\frac{\theta}{2}\cos\frac{\Phi}{2} - (p-q)\sin\frac{\theta}{2}\sin\frac{\Phi}{2}\right]\cos\chi\,. \tag{18}$$

The last three terms in Eq. (18) are the Josephson coupling energy (4) in terms of the variables θ, Φ, and χ. The minimization of U with respect to χ gives the expression (13) for $\cos\chi$, with ϕ replaced by Φ. At given values of the control parameters I and Φ^e, the relations (16) and (17) (together with Eq. (13)) determine the set of possible states of the system $\{\theta, \Phi\}$, among which we should choose those that correspond to the local minima of the potential U, Eq. (18).

Let us consider the effect of the magnetic flux state of the ring on the behavior of the current-driven junction. The critical current of the junction, I_c, depends on the applied magnetic flux Φ^e. In the simplest case of small self-inductance $\mathcal{L} << 1$, we can neglect the difference between Φ and Φ^e in expression (16). The maximal value of the supercurrent I (16) (with Φ replaced by Φ^e) as a function of Φ^e, $I_{\max}(\Phi^e)$, is shown in Fig. 9. This

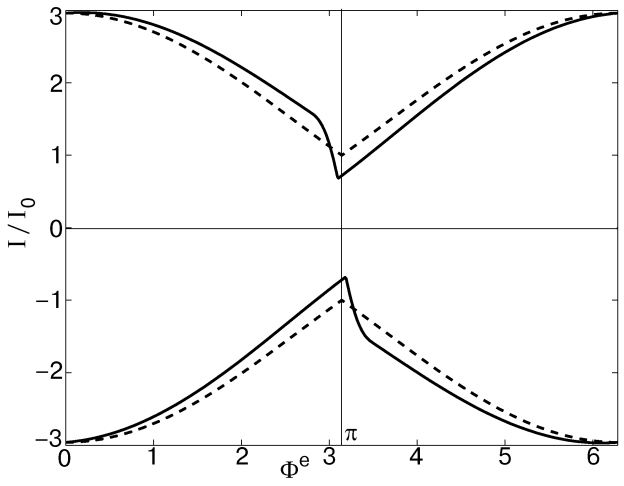

Fig. 9. The steady-state domain for a mesoscopic four-terminal SQUID in the plane (I, Φ^e) of the control parameters (solid line). The dashed line corresponds to conventional four-terminal SQUIDs.

curve determines the boundary of the steady-state domain in the (I, Φ^e) plane. The function $I_{\max}(\Phi^e)$ is 2π periodic, but due to the terms proportional to $p-q$ in Eq. (16), it is not invariant under the transformation $\Phi^e \to -\Phi^e$. The symmetry is restored if we simultaneously change Φ^e to $-\Phi^e$ and I to $-I$. Note that in the conventional case ($p = q$) the boundary of the steady-state domain $I_{\max}(\Phi^e)$ is symmetric with respect to the axes (I, Φ^e) (dashed line in Fig. 9). Thus the critical current I_c in the transport current circuit, for a given direction of the current, depends on the sign of the magnetic flux in the ring. For finite values of self-inductance $\mathcal{L}$,

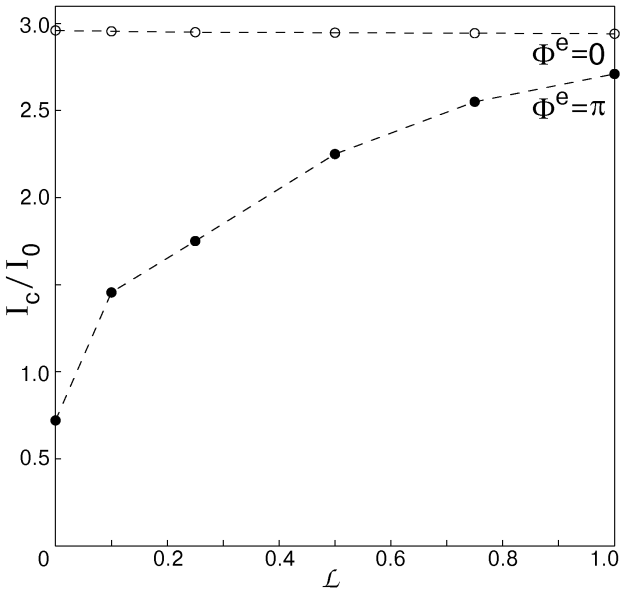

Fig. 10. The critical current, I_c, between the superconductors S_1 and S_2, as a function of $\mathcal{L}$ for $\Phi^e = 0$ and π.

equations (16) and (17) must be treated self-consistently. The critical current I_c as function of $\mathcal{L}$ is shown in Fig. 10 for two values of external flux, $\Phi^e = 0$ and $\Phi^e = \pi$.

Outside the steady-state domain, the stationary solutions for (θ, Φ) are absent and system goes to the nonstationary resistive regime. The simple generalization of Eqs. (16), (17) in the framework of the heavily damped resistively shunted junction (RSJ) model [3] leads to equations (see [7]):

$$\frac{d\theta}{dt} = I - \sin\theta - \left[(p+q)\sin\frac{\theta}{2}\cos\frac{\Phi}{2} + (p-q)\cos\frac{\theta}{2}\sin\frac{\Phi}{2}\right]\cos\chi\,, \tag{19}$$

$$\frac{d\Phi}{dt} = \frac{\Phi^e - \Phi}{\mathcal{L}} - \sin\Phi - \frac{1}{\kappa}\left[(p+q)\sin\frac{\Phi}{2}\cos\frac{\theta}{2} + (p-q)\cos\frac{\Phi}{2}\sin\frac{\theta}{2}\right]\cos\chi\,, \tag{20}$$

$$\frac{d\chi}{dt} = -\sin\chi\left[(p+q)\cos\frac{\Phi}{2}\cos\frac{\theta}{2} - (p-q)\sin\frac{\Phi}{2}\sin\frac{\theta}{2}\right]. \tag{21}$$

They can also be presented in the form

$$\dot\theta = -\frac{\partial U}{\partial\theta}\,, \quad \dot\Phi = -\frac{\partial U}{\partial\Phi}\,, \quad \dot\chi = -\frac{1}{2}\frac{\partial U}{\partial\chi}\,, \tag{22}$$

where the potential U is defined in Eq. (18). The voltages between different terminals are related to the time derivatives of the phase differences

$$V_{21} = \dot\theta\,, \quad V_{34} = \dot\Phi\,, \quad \frac{1}{2}(V_{13} + V_{24}) = \dot\chi\,. \tag{23}$$

The time and the voltage are measured in the units of e/I_0 and $\hbar I_0/2e^2$, respectively. Note that, in spite of the equilibrium state, the dynamical variable χ relates to an observable quantity. Its time derivative determines the voltage between the ring and the transport circuit. The features of the dynamical behavior of the mesoscopic 4-terminal SQUID are again affected by the terms proportional to $(p-q)$, i.e., by nonlocal coupling. The current–voltage characteristics in the transport channel, $V(I)$ (the time averaged voltage V_{21} (23)), can be obtained by numerical solution of the coupled system of nonlinear differential equations (20)–(22). As well as the critical current I_c, the voltage $V(I)$ in an applied magnetic flux Φ^e depends on the sign of Φ^e, i.e., on the direction of the external magnetic field. A full dynamical description of the mesoscopic four-terminal SQUID requires a more rigorous approach than the RSJ model and will be the subject of a separate investigation.

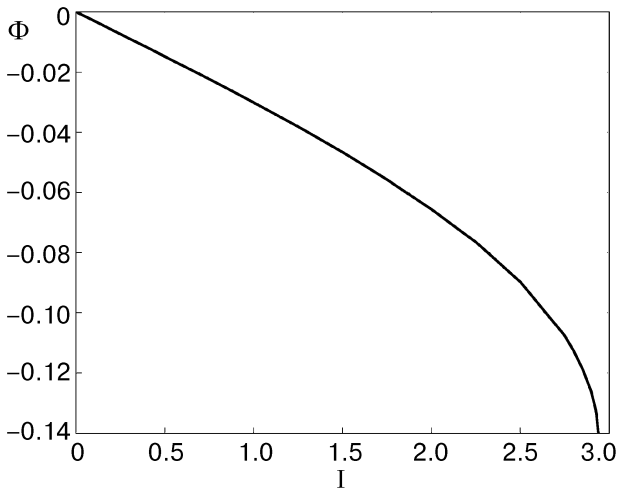

Fig. 11. The flux induced inside the ring as a function of the transport current I. $\mathcal{L} = 1$, $\Phi^e = 0$.

In accordance with the stationary (16), (17) or dynamical equations (19)–(21) for θ and Φ the opposite effect for the influence of transport current circuit on the flux states in the ring takes place. In particular, a current I produces a flux Φ in the ring even in stationary case and in the absence of external flux Φ^e. This effect is proportional to $(p-q)$ and is absent in the conventional case. In Fig. 11 we plot the magnetic flux Φ induced in the ring as a function of the transport current I in the case $\Phi^e = 0$.

A special interest is the existence of bistable states in the system described by the potential (18). We emphasize that, in contrast to the usual SQUID, bistable states occur for any inductance $\mathcal{L}$, even for $\mathcal{L} < 1$ [5]. We will analyze the dependence of these states on the control parameters I and Φ^e in Article II, when the design of the four-terminal qubit will be studied.

5. Conclusions

We have demonstrated that in ballistic four-terminal Josephson junctions the coherent anisotropic superposition of the macroscopic wave functions of the superconductors in the normal region produces the formation of phase slip lines ($2D$ analogs to phase slip centers) and time-reversal symmetry

breaking $2D$ vortex states in it, as well as such effects as phase dragging and magnetic flux transfer. We have calculated the phase-dependent tunneling density of Andreev states in this region as well.

The degree to which the nonlocality of the mesoscopic transport is manifested depends on the characteristics of the system and is most pronounced in the ballistic case [20]. The ballistic four-terminal junctions considered here demonstrate several specific effects absent in the diffusive limit [4–6]: phase dragging, time-reversal symmetry breaking ($I(\theta) \neq I(-\theta)$), Eq. (14)), and the vortex formation. The latter can mimic the behavior of S–N–S junctions with unconventional superconductors [21]. It has indeed the same origin in the direction-dependent phase of the superconducting order parameter induced in the normal part of the system, though not due to the intrinsic phase difference between different directions in a superconductor. This actually allows us more freedom in controlling the behavior of the junction, which will be exploited in the qubit design based on such a junction in the following paper. The time-reversal symmetry breaking can be also used for direction-sensitive detection of weak magnetic fluxes.

It will be instructive to investigate the role played by finite elastic scattering in the system and look for the analogs of zero bound states, found at surfaces/interfaces of unconventional superconductors (for a review see [22]). This, as well as the vortex dynamics in the system, will be the subject of our further research.

We thanks R. de. Bruyn Ouboter for his stimulating interest in this work. One of the authors, A. N. O., would like to acknowledge D-Wave Systems Inc. (Vancouver) for hospitality and support of this research.

Appendix

Junction with arbitrary γ's

The Josephson energy of the mesoscopic four-terminal junction, normalized to

$$(\hbar/2e)\pi\Delta_0^2(T)/4eT_c ,$$

is expressed by

$$E_J = -\gamma_{12}\cos\theta - \gamma_{34}\cos\phi + E_{\text{coupl}} , \quad \text{(A.1)}$$

with the coupling energy E_{coupl} given by

$$E_{\text{coupl}} = -\gamma_{13}\cos\left(\frac{-\theta-\phi}{2}+\chi\right) - \gamma_{14}\cos\left(\frac{-\theta+\phi}{2}+\chi\right) -$$
$$-\gamma_{23}\cos\left(\frac{\theta-\phi}{2}+\chi\right) - \gamma_{24}\cos\left(\frac{\theta+\phi}{2}+\chi\right) =$$
$$= -(A\cos\chi + B\sin\chi) , \quad \text{(A.2)}$$

where

$$A = (\gamma_{13}+\gamma_{24})\cos\left(\frac{\theta+\phi}{2}\right) + (\gamma_{14}+\gamma_{23})\cos\left(\frac{\theta-\phi}{2}\right), \quad \text{(A.3)}$$

$$B = (\gamma_{13}-\gamma_{24})\sin\left(\frac{\theta+\phi}{2}\right) + (\gamma_{14}-\gamma_{23})\sin\left(\frac{\theta-\phi}{2}\right).$$

Minimizing with respect to χ, we find the minimum to be

$$E_{\text{coupl}} = -\sqrt{A^2+B^2} , \quad \chi = \cos^{-1}\left(\frac{A}{\sqrt{A^2+B^2}}\right). \quad \text{(A.4)}$$

After some manipulations we find

$$E_{\text{coupl}} = -[\gamma_{13}^2+\gamma_{23}^2+\gamma_{14}^2+\gamma_{24}^2 + 2(\gamma_{13}\gamma_{14}+\gamma_{23}\gamma_{24})\times$$
$$\times\cos\phi + 2(\gamma_{13}\gamma_{23}+\gamma_{14}\gamma_{24})\cos\theta + 2(\gamma_{13}\gamma_{24}+\gamma_{14}\gamma_{23})\times$$
$$\times\cos\theta\cos\phi - 2(\gamma_{13}\gamma_{24}-\gamma_{14}\gamma_{23})\sin\theta\sin\phi]^{1/2} . \quad \text{(A.5)}$$

The last term in the bracket in (A.5) vanishes when $\det(\hat{\gamma}_{\text{coupl}}) = 0$. In that case the current $I(\theta, \phi)$ will be zero at $\theta = 0$. On the other hand, if $\det(\hat{\gamma}_{\text{coupl}}) \neq 0$, then $I(\theta, \phi) \neq 0$ when $\theta = 0$. This is a signature of the phase dragging effect.

In a four-terminal junction with microbridges near T_c one has $\gamma_{ij} \sim 1/R_i R_j$. In that case the last term in (A.5) will vanish and E_{coupl} factorizes:

$$E_{\text{coupl}} \sim -\left[\left(\frac{1}{R_1}-\frac{1}{R_2}\right)^2 + \frac{4\cos^2(\theta/2)}{R_1R_2}\right]^{1/2}\times$$
$$\times\left[\left(\frac{1}{R_3}-\frac{1}{R_4}\right)^2 + \frac{4\cos^2(\phi/2)}{R_3R_4}\right]^{1/2} . \quad \text{(A.6)}$$

In particular, when $R_1 = R_2$ and $R_3 = R_4$ we find

$$E_{\text{coupl}} \sim -\frac{4}{R_1R_3}\left|\cos\frac{\theta}{2}\right|\left|\cos\frac{\phi}{2}\right| , \quad \text{(A.7)}$$

which is what one obtains from Ginzburg–Landau calculation.

In a mesoscopic four-terminal junction with parallel implementation on the other hand, we have $\gamma_{13} = \gamma_{24}$ and $\gamma_{14} = \gamma_{23}$. This leads to $B = 0$ and therefore

$$E_{\text{coupl}} = -|A|, \quad \cos\chi = \text{sign}\,(A), \qquad \text{(A.8)}$$

which gives $\chi = 0$ or π. Notice that in the general case of (A.4), χ can take values other than 0 and π.

1. K. K. Likharev, *Rev. Mod. Phys.* **51**, 101 (1979).
2. I. O. Kulik, A. N. Omelyanchouk, and E. A. Kel'man, *Fiz. Nizk. Temp.* **3**, 1107 (1977) [*Sov. J. Low Temp. Phys.* **3**, 537 (1977)].
3. A. Barone and G. Paterno, *Physics and Applications of the Josephson Effect*, Wiley, New York (1982).
4. E. D. Vol and A. N. Omelyanchouk, *Fiz. Nizk. Temp.* **20**, 107 (1994) [*Low Temp. Phys.* **20**, 87 (1994)].
5. R. de Bruyn Ouboter, A. N. Omelyanchouk, and E. D. Vol, *Physica* **B205**, 153 (1995); *ibid*. **239**, 203 (1997).
6. L. G. Aslamazov and A. I. Larkin, *JETP Lett.* **9**, 87 (1969).
7. R. de Bruyn Ouboter and A. N. Omelyanchouk, *Superlatt. and Microstruct.* **23**, 1005 (1999).
8. B. J. Vleeming, *Ph. D. Thesis*, Leiden University (1998).
9. I. O. Kulik, *Sov. Phys. JETP* **30**, 944 (1970).
10. I. O. Kulik and A. N. Omelyanchouk, *Fiz. Nizk. Temp.* **4**, 296 (1978) [*Sov. J. Low Temp. Phys.* **4**, 142 (1978)]; C. W. J. Beenakker and H. van Houten, *Phys. Rev. Lett.* **66**, 3056 (1991).
11. Y. Imry, *Introduction to Mesoscopic Physics*, Oxford, New York (1997).
12. A. F. Andreev, *Sov. Phys. JETP* **19**, 1228 (1964).
13. J. P. Heida, B. J. van Wees, T. M. Klapwijk, and G. Borghs, *Phys. Rev.* **B57**, R5618 (1998).
14. V. Barzykin and A. M. Zagoskin, *Superlatt. and Microstruct.* **25**, 797 (1999).
15. U. Ledermann, A. L. Fauchére, and G. Blatter, *Phys. Rev.* **B59**, R9027 (1999).
16. Malek Zareyan and A. N. Omelyanchouk, *Fiz. Nizk. Temp.* **25**, 240 (1999) [*Low Temp. Phys.* **25**, 175 (1999)].
17. A. N. Omelyanchouk and Malek Zareyan, *Physica* **B291**, 81 (2000).
18. M. Buttiker, *Phys. Rev. Lett.* **37**, 1761 (1986).
19. G. Eilenberger, *Z. Phys.* **214**, 195 (1968).
20. I. O. Kulik, A. N. Omel'yanchuk, and R. I. Shekhter, *Fiz. Nizk. Temp.* **3**, 1543 (1977) [*Sov. J. Low Temp. Phys.* **3**, 740 (1977)].
21. A. Huck, A. van Otterlo, and M. Sigrist, *Phys. Rev.* **B56**, 14163 (1997); A. M. Zagoskin, *J. Phys.: Condensed Matter* **9**, L419 (1997); *cond-mat/9903170* (1999).
22. S. Kashiwaya and Y. Tanaka, *Rep. Progr. Phys.* **63**, 1641 (2000).